frontiers | Frontiers in Chemistry

TYPE Original Research
PUBLISHED 16 November 2022
DOI 10.3389/fchem.2022.1025135

OPEN ACCESS

EDITED BY
Israel Fernandez,
Complutense University of Madrid, Spain

REVIEWED BY
Miquel Solà,
University of Girona, Spain
Cina Foroutan-Nejad,
Institute of Organic Chemistry (PAN), Poland

*CORRESPONDENCE
Gui-Juan Cheng,
guijuancheng@foxmail.com

†These authors have contributed equally to this work

SPECIALTY SECTION
This article was submitted to Theoretical and Computational Chemistry, a section of the journal Frontiers in Chemistry

RECEIVED 22 August 2022
ACCEPTED 20 September 2022
PUBLISHED 16 November 2022

CITATION
Zhou M, Wang T and Cheng G-J (2022), Mechanistic insights into reductive deamination with hydrosilanes catalyzed by $B(C_6F_5)_3$: A DFT study. *Front. Chem.* 10:1025135. doi: 10.3389/fchem.2022.1025135

Mechanistic insights into reductive deamination with hydrosilanes catalyzed by $B(C_6F_5)_3$: A DFT study

Miaomiao Zhou[1,2†], Ting Wang[1†] and Gui-Juan Cheng[1,3,4*]

[1]Warshel Institute for Computational Biology, School of Medicine, The Chinese University of Hong Kong (Shenzhen), Shenzhen, China, [2]Department of Chemistry, City University of Hong Kong, KowloonTong, Hong Kong SAR, China, [3]School of Life and Health Sciences, School of Medicine, The Chinese University of Hong Kong (Shenzhen), Shenzhen, China, [4]Shenzhen Key Laboratory of Steroid Drug Development, School of Medicine, The Chinese University of Hong Kong (Shenzhen), Shenzhen, China

Selective defunctionalization of synthetic intermediates is a valuable approach in organic synthesis. Here, we present a theoretical study on the recently developed $B(C_6F_5)_3$/hydrosilane-mediated reductive deamination reaction of primary amines. Our computational results provide important insights into the reaction mechanism, including the active intermediate, the competing reactions of the active intermediate, the role of excess hydrosilane, and the origin of chemoselectivity. Moreover, the study on the substituent effect of hydrosilane indicated a potential way to improve the efficiency of the reductive deamination reaction.

KEYWORDS

$B(C_6F_5)_3$, reductive deamination, reaction mechanism, substituent effect, DFT

Introduction

In the search for renewable alternatives, biomass feedstock is usually a promising sustainable carbon source to produce fuels, chemicals, and materials. In general, biomass-derived feedstocks, such as sugars, alcohol, phenol, and amines, are over-functionalized. Therefore, defunctionalization has become an important way to produce useful downstream chemicals, which has attracted wide attention. (Huber et al., 2006; Corma et al., 2007; Zhou et al., 2011; Zhang et al., 2017). Over last 2 decades, the deoxygenation of alcohols or derivatives has been well developed to access simple hydrocarbons. (Adlington et al., 1976; Doyle et al., 1976; Orfanopoulos and Smonou, 1988; Yasuda et al., 2001; Nimmagadda and McRae, 2006; McLaughlin et al., 2013; Dai and Li, 2016). Conversely, although amines are also one of the most common feedstock chemicals accessible by biomass conversion, the deaminative transformation of amines is poorly developed, which highlights great challenges, particularly in the development of deaminative strategies for alkyl amines and primary amines to construct C–X (X = C, O, S, B, P, H, etc.) bonds.

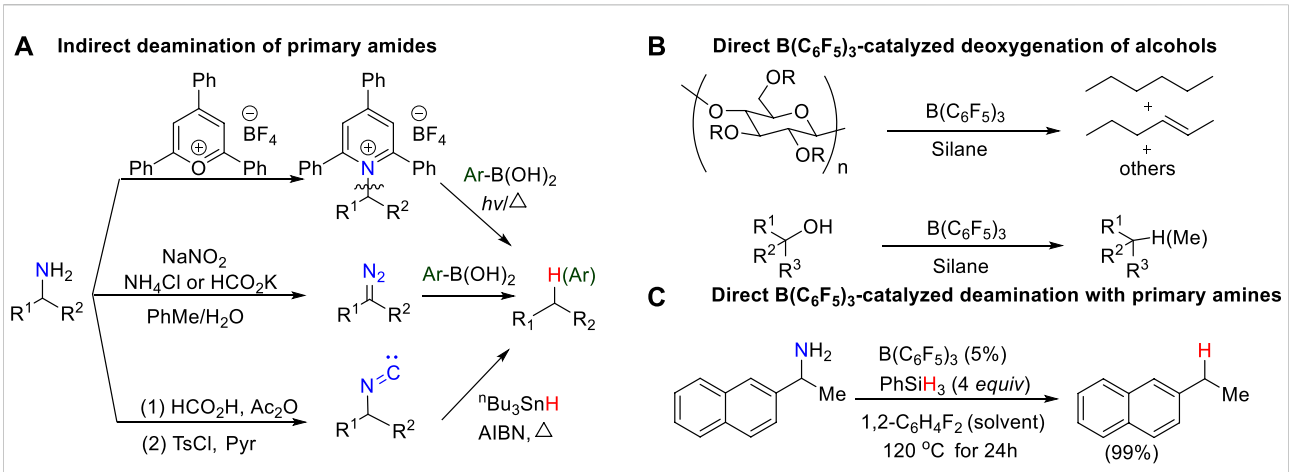

SCHEME 1
(A) Indirect deamination of primary amine; **(B)** Direct $B(C_6F_5)_3$-catalyzed deoxygenation of primary alcohols; **(C)** Direct $B(C_6F_5)_3$-catalyzed deamination of primary amines.

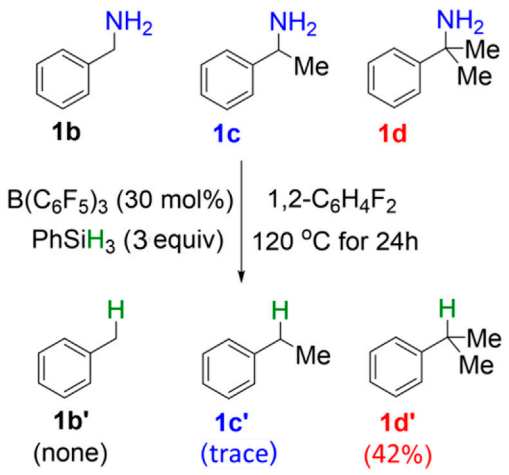

SCHEME 2
Reactivity study on $B(C_6F_5)_3$-catalyzed reductive deamination with equimolar mixture of benzylamines **(1b**, **1c**, **1d)** and $PhSiH_3$.

Deaminases, such as L-amino acid deaminases (LAAD), are essential biocatalyst in living cells. In the human body, deamination, as a common metabolic process, usually takes place to break down amino acids for the generation of their corresponding α-keto acids and ammonia by deaminases, involving in nucleotide sequence, immunity and cancer. (Massad et al., 1995; Petersen-Mahrt et al., 2009; Vesely et al., 2012; Molla et al., 2017; Nshimiyimana et al., 2019). In contrast, deamination in laboratory is very rare and difficult. Although the challenges are daunting, systematic efforts toward deamination of primary amines have recently begun to emerge, and some progress has been made. Earlier work on C–NH_2 bond activation usually requires to pre-activate primary amines into reactive intermediates, such as active pyridinium salts (Katritzky salts) (Hu et al., 2018; Ni et al., 2019; Wang et al., 2019; Correia et al., 2020; Pang et al., 2020), electron-rich diazos (Mitsuhashi et al., 2000; Geoffroy et al., 2001; Barluenga et al., 2009; Peng et al., 2009; Wu et al., 2014), and isonitrile compounds (Barton et al., 1980; Barton et al., 1992), for further deamination, which results in a more complicated and expensive reaction process (Scheme 1A). Based on the principles of green chemistry and sustainable development, the direct activation of C–N bond of primary amines without pre-activation affords a very attractive approach to obtain valuable functionalized building blocks even though it is more challenging.

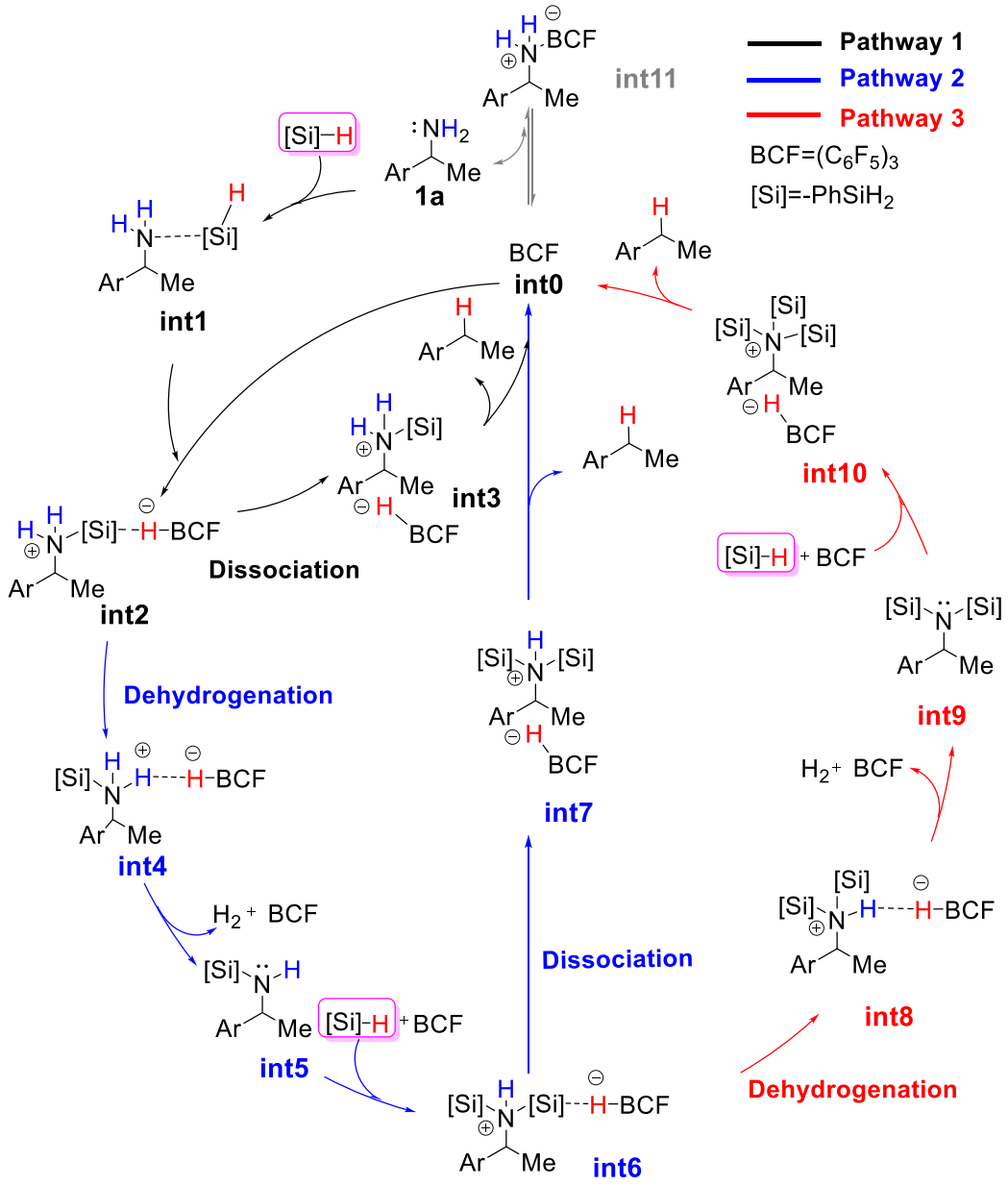

FIGURE 1
The proposed catalytic cycle for $B(C_6F_5)_3$-catalyzed reductive deamination with hydrosilanes.

The combination of $B(C_6F_5)_3$ and hydrosilanes was recently discovered for selective deoxygenations of 1,2-diols and polyols by the Gagné (Adduci et al., 2014; Adduci et al., 2015; Bender et al., 2016a; Bender et al., 2016b; Seo and Gagné, 2018; Seo et al., 2019), Morandi (Drosos and Morandi, 2015; Nikolaos Drosos and Morandi, 2015; Drosos et al., 2016), Yamamoto (Gevorgyan et al., 1999; Gevorgyan et al., 2000; Gevorgyan et al., 2001), and Oestreich group (Chatterjee et al., 2017; Fang and Oestreich, 2020a; Richter and Oestreich, 2021) (Scheme 1B). However, the reaction of $B(C_6F_5)_3$ and hydrosilanes with amines generally does not give deamination product; instead, it affords N-silylation product which is formed *via* $B(C_6F_5)_3$-catalyzed dehydrogenative coupling of amines and hydrosilanes. (Hermeke et al., 2013; Greb et al., 2014; Zhang et al., 2018; Zhou et al., 2020). Recently, the Oestreich group reported the first metal-free, $B(C_6F_5)_3$/hydrosilane-mediated deamination reaction of primary amines, which was a breakthrough for the direct C–NH_2 bond defunctionalization (Scheme 1C). (Fang and Oestreich, 2020b) Their study showed that the amount of silane reagent is essential to the reaction: 4 equivalents of $PhSiH_3$ were required to obtain

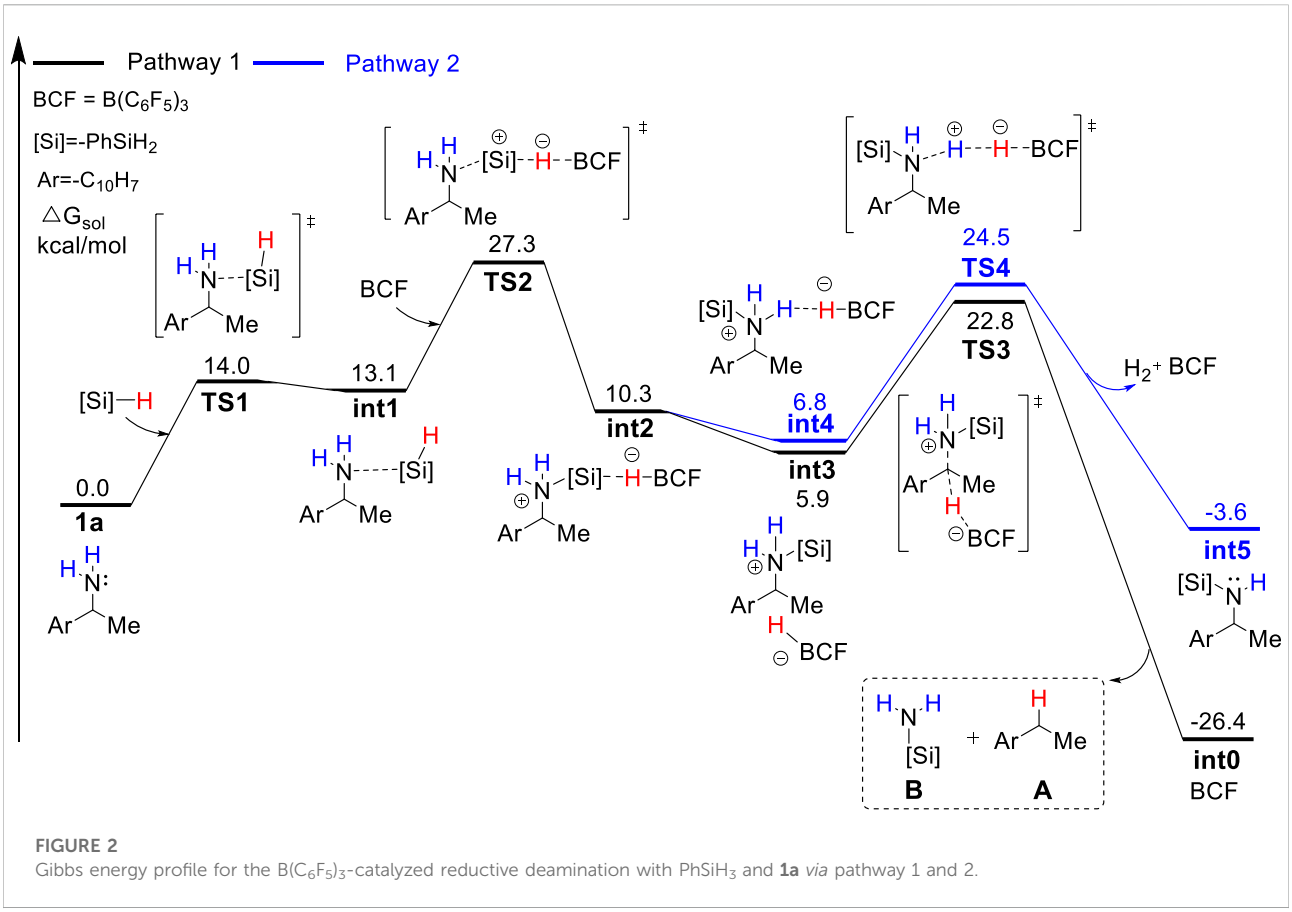

FIGURE 2
Gibbs energy profile for the $B(C_6F_5)_3$-catalyzed reductive deamination with $PhSiH_3$ and **1a** *via* pathway 1 and 2.

high yields, and less $PhSiH_3$ would result in poor yields. Additionally, they found the substitution degree of benzylamines significantly affects the reactivity. But the role of excess hydrosilane and substituent effect on reactivity remain elusive. In addition, the stoichiometric experiments indicated the existence of silylammonium borohydride which was proposed to undergo C–N cleavage to afford deamination product. However, it is unclear which species among mono-, di-, or tri-silylammonium borohydrides (i.e., **int2**, **int6** or **int10** shown in Figure 1) is the active intermediate. Moreover, it remains unknown how does deamination compete over the dehydrogenative coupling to successfully afford desired product. A deeper understanding of the reaction mechanism may provide useful information for the optimization and development of deamination reactions.

Our group is particularly interested in the diverse catalytic capabilities of $B(C_6F_5)_3$ system. In previous computational study on $B(C_6F_5)_3$-catalyzed deoxygenation of polyols with silanes, we rationalized the special role of the cyclic siloxane intermediate in promoting reactivity and selectivity, as well as the different product distributions obtained with different silanes. (Drosos et al., 2017; Cheng et al., 2018).

Herein, we disclose the reaction mechanism of $B(C_6F_5)_3$-catalyzed deamination by theoretical studies, thereby expanding the understanding of $B(C_6F_5)_3$ catalytic system. The present work provides a detailed mechanistic picture for $B(C_6F_5)_3$-catalyzed deamination reaction, unveils the role of excess hydrosilane, and explains the substituent effect on reactivity.

Computational details

All the calculations were performed with Gaussian 16 (Frisch et al., 2016) package. All molecular geometries were optimized with B3LYP-D3/def2SVP method in gas phase. (Lee et al., 1988; Schafer et al., 1992; Becke, 1993; Schafer et al., 1994; Grimme et al., 2011). Optimized geometries were verified by frequency computations as minima (zero imaginary frequencies) or transition state (a single imaginary frequency) at the same level of theory. The transition states (TSs) were also confirmed by viewing normal mode vibrational vector and by intrinsic reaction coordinate (IRC) calculation. (Gonzalez and Gonzalez, 1990). All the single point energy calculations in solution phase were carried out by SMD(Marenich et al.,

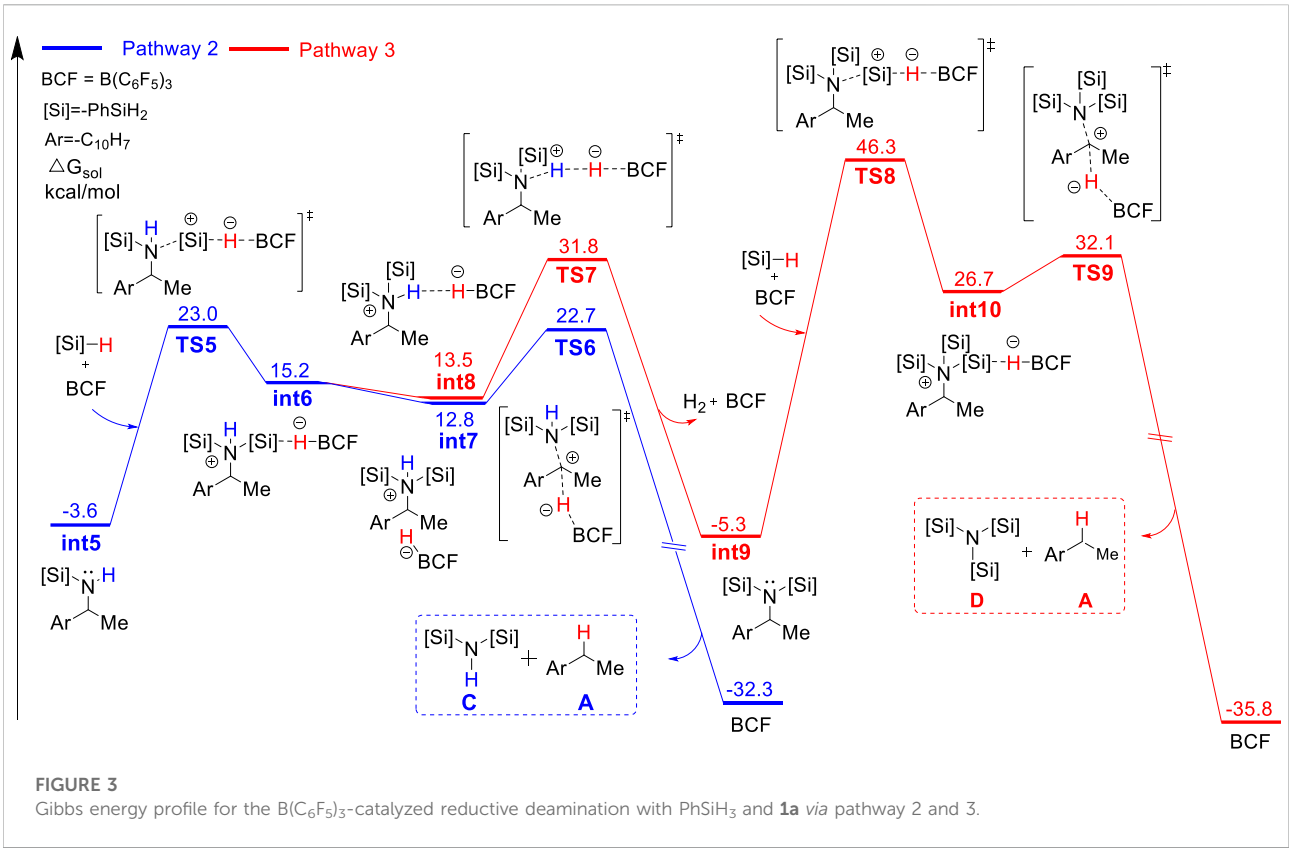

FIGURE 3
Gibbs energy profile for the $B(C_6F_5)_3$-catalyzed reductive deamination with $PhSiH_3$ and **1a** *via* pathway 2 and 3.

2009) model with 1,2-diflurobenzene as the solvent and B3LYP-D3 method with the def2-TZVP basis set. All of Gibbs energies were corrected at 393.15K. Both relative Gibbs energies and electronic energies were reported in kcal/mol. The 3D structures were generated by CYLview. (Legault, 2009). The conformational space of the system has been extensively explored manually by rotating the torsional angles of the molecule and automatically by using Crest program. (Grimme, 2019).

Results and discussion

Reaction mechanism of $B(C_6F_5)_3$-catalyzed reductive deamination with $PhSiH_3$ and 1a

As discussed in the introduction, silylammonium borohydride was detected in the stoichiometric experiment and proposed to undergo C–N cleavage to form deamination product. Because it is unknown which one among mono-, bi-, and tri-silylammonium borohydrides (i.e., **int2**, **int6** or **int10** shown in Figure 1) is the active intermediate that leads to deamination product, we calculated three possible pathways that involve different silylammonium borohydrides. As shown in Figure 2, the reaction is initiated by the association of substrate **1a** with one $PhSiH_3$. This step needs to overcome a Gibbs energy barrier of 14.0 kcal/mol (**TS1**), generating a thermodynamically unstable amine-silane complex **int1**. Then, the Lewis acid $B(C_6F_5)_3$ abstracts a hydride from **int1**, which is accompanied by the N–Si bond formation to afford the monosilylammonium borohydride species (**int2**). The activation energy barrier for the silylation process is 27.3 kcal/mol (**TS2**). The monosilylammonium borohydride intermediate then undergoes C–N bond dissociation (pathway 1), where borohydride $(C_6F_5)_3BH^-$ acts as a nucleophile to attack the benzylic carbon of silylammonium moiety *via* an S_N2-*type* transition state (**TS3**) to afford the desired deamination product **A** and monosilazane **B**. The rate-determining step of pathway one is the silylation step (**TS2**) and overall reaction barrier is 27.3 kcal/mol.

Alternatively, the monosilylammonium borohydride intermediate may occur dehydrogenative reaction (pathway 2, blue color), in which $(C_6F_5)_3BH^-$ accepts a proton from the amine group (**TS4**), which releases a H_2 molecule, $B(C_6F_5)_3$ and mono-silylated amine **int5**. The Gibbs energy barrier of **TS4** is 1.7 kcal/mol higher than that of **TS3**, indicating that the monosilylammonium borohydride intermediate prefers C–N dissociation than dehydrogenation. Follow the dehydrogenative step, **int5** further reacts with another $PhSiH_3$ molecule and $B(C_6F_5)_3$ catalyst to give the disilylammonium borohydride

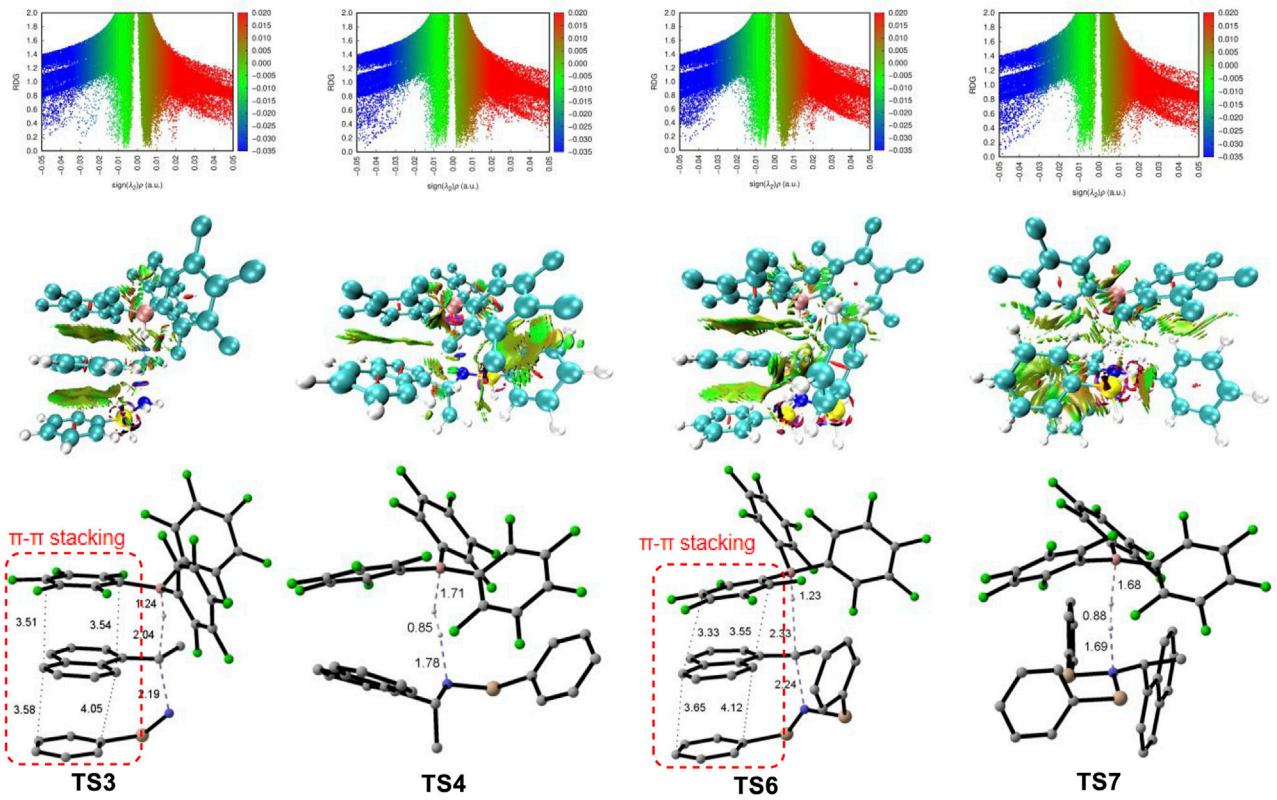

FIGURE 4
Top: Overlapping troughs in s(ρ) plots can be distinguished when sign (λ_2)ρ is used as the ordinate. Favorable interactions appear on the left, unfavorable on the right, and van der Waals near zero; Medium: NCI surfaces of **TS3**, **TS4**, **TS6 and TS7** correspond to s = 0.5 au and a colour scale of $-0.05 < \rho < 0.05$ au for SCF densities; Bottom: structures of **TS3**, **TS4**, **TS6 and TS7** (Non-reacting hydrogen atoms are omitted for clarity).

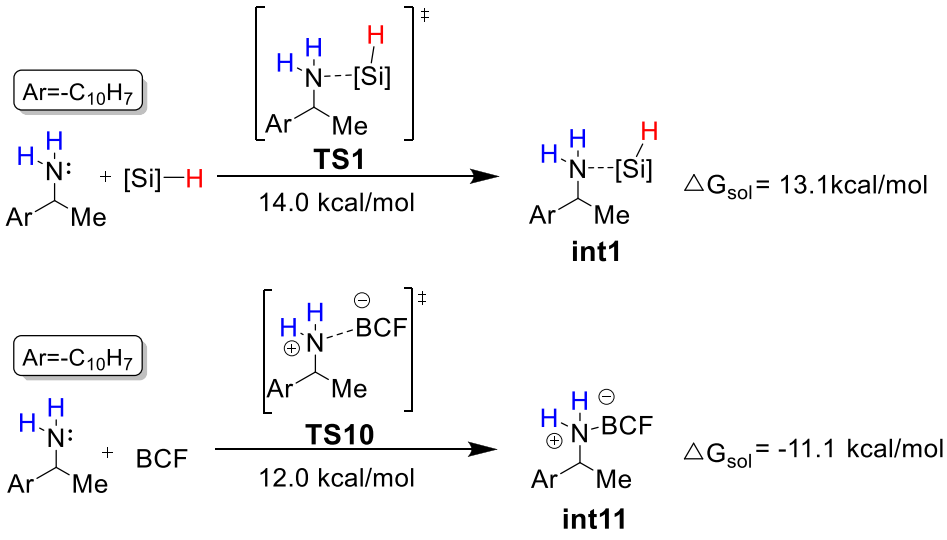

FIGURE 5
Competition between the formation of **int1** and **int11**. BCF = $B(C_6F_5)_3$; [Si] = $-PhSiH_2$.

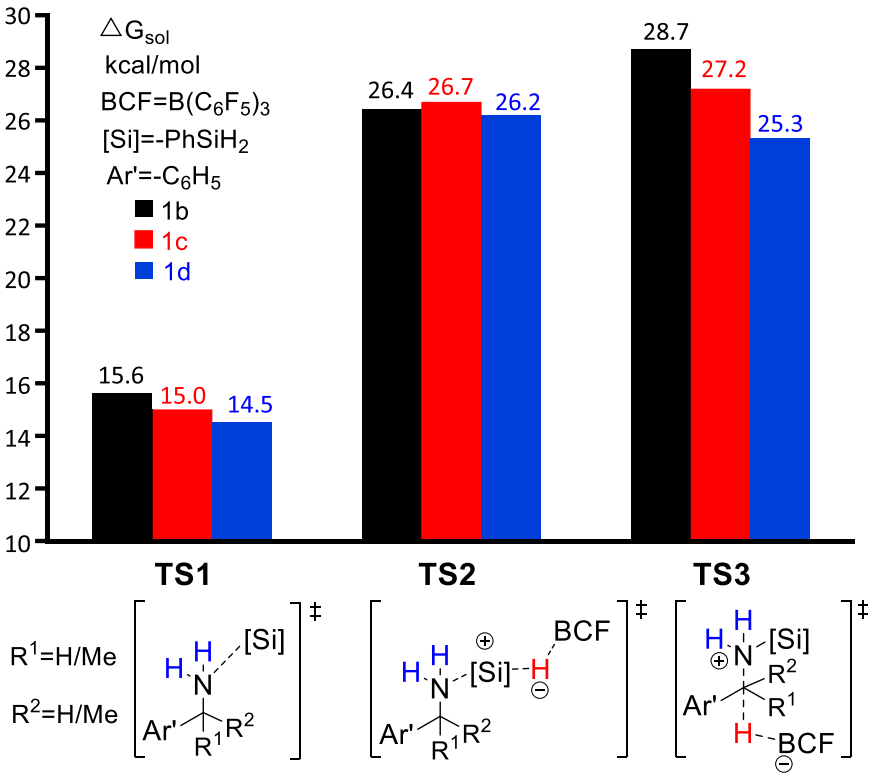

FIGURE 6
Gibbs energy of transition states **TS1**, **TS2**, and **TS3** for different substrates.

intermediate, **int6** (Figure 3). Like the monosilylammonium borohydride, the disilylammonium borohydride intermediate can undergo an *S_N2-type* C–N cleavage (**TS6**, $\Delta G^{\ddagger}$ = 26.3 kcal/mol) to yield the deamination species **A** and disilazane **C**, completing pathway 2. Pathways one and two bifurcate at the monosilylammonium borohydride intermediate and pathway two is less favorable since the monosilylammonium borohydride intermediate favors C–N dissociation.

In the alternative pathway 3 (in red color), the dehydrogenation of disilylammonium borohydride intermediate *via* **TS7** ($\Delta G^{\ddagger}$ = 35.4 kcal/mol) releases one H_2 molecule and a disilyated amine (**int9**). **int9** then reacts with another molecule of $PhSiH_3$ and $B(C_6F_5)_3$ for further silylation. The silylation step proceeds *via* a very high energy barrier transition state, **TS8**, ($\Delta G^{\ddagger}$ = 51.6 kcal/mol) and yields a highly unstable trisilylammonium borohydride species **int10**. Finally, the **C–N** dissociation of the trisilylammonium borohydride *via* **TS9** releases product **A** and trisilazane **D**. In summary, the computational results suggest the direct C–N dissociation of the monosilylammonium borohydride to generate monosilazane and deamination product (pathway 1) is the most favorable pathway for this reductive deamination reaction. The first silylation step *via* **TS2** is the rate-limiting step and the overall energy barrier is 27.5 kcal/mol. Moreover, the TSs of dehydrogenation of both mono- and di-silylammonium borohydride are higher in energy than their corresponding TSs of C–N dissociation energy (**TS3** vs. **TS4** and **TS6** vs. **TS7**), suggesting the deamination is more favorable than dehydrogenation reaction which is consistent with experimental results. The lower activation barrier of deamination can be attributed to the weaker bond strength of C–N bond compared with the N–H bond. The calculated bond dissociation energy of C–N bond is lower than that of N–H bond by 8.5 and 13.2 kcal/mol for mono- and di-silylammonium borohydride, respectively (Supplementary Table S1). Thus, the C–N bond is easier to be cleavage than the N–H bond. In addition, well-ordered π-π stacking interactions between the naphthyl ring of substrate, the phenyl ring of silane and the pentafluorophenyl group of the catalyst were identified in **TS3** and **TS6** (Figure 4), which help to stabilize the deamination TSs. The NCI analysis (Humphrey et al., 1996; Lu and Chen, 2012) supports the existence of attractive π-π stacking interactions in **TS3** and **TS6**.

Based on the theoretical calculation, the most favorable pathway (i.e., pathway 1) only consumes one equivalent of $PhSiH_3$ to afford the deamination product **A**, which contradicts with the experimental observation that four equivalents of $PhSiH_3$ are required to achieve good yields. Because both $PhSiH_3$ and $B(C_6F_5)_3$ are Lewis acids, we envision that $PhSiH_3$ and $B(C_6F_5)_3$

10.3389/fchem.2022.1025135

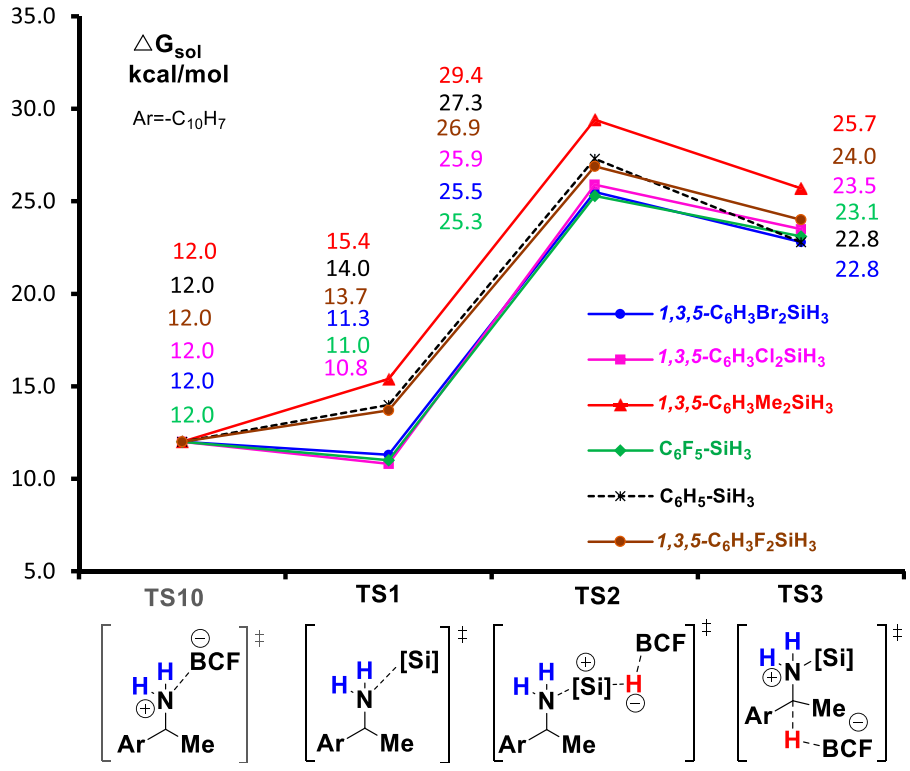

FIGURE 7
The $B(C_6F_5)_3$-catalyzed reductive deamination with different hydrosilanes.

may compete to bind with the amine substrate to form amine-silane ([N-Si]) and amine-boron ([N-B]) Lewis adducts, respectively. As shown in Figure 5, the binding of **1a** with $B(C_6F_5)_3$ has a Gibbs energy barrier lower by 2.0 kcal/mol than with $PhSiH_3$ and leads to a very stable [N-B] Lewis adduct **int11** (ΔG^o = −11.1 kcal/mol). Thus, computational results suggest that the formation of [N–B] Lewis adduct (**int11**) is kinetically and thermodynamically more favorable than [N–Si] Lewis adduct (**int1**). The favorable formation of [N–B] Lewis adduct can be attributed to the stronger Lewis acidity of $B(C_6F_5)_3$. Frontier molecular orbital analysis supports that $B(C_6F_5)_3$ is a much stronger Lewis acid than $PhSiH_3$ and thus easier to accept a lone pair electron from **1a** (Supplementary Figure S2).

The computational results demonstrate that when $B(C_6F_5)_3$ and $PhSiH_3$ were added with a ratio of 1:1, the amine substrate prefers to bind with $B(C_6F_5)_3$ and form a very stable Lewis adduct (**int11**) which is the resting state of catalyst and substrate. Taking the resting state **int11** as the start point for the deamination reaction, the overall reaction barrier is as high as 38.6 kcal/mol (**int11** to **TS2**), which is difficult to overcome. This result is in line with the experimental observation that **int11** rather than the deamination product was obtained as main product in the stoichiometric experiments with stepwise addition of $B(C_6F_5)_3$ and $PhSiH_3$.

In the catalytic reaction with 20% mol of $B(C_6F_5)_3$, the use of four equivalents of $PhSiH_3$ afforded deamination product as main product. We speculate this is related to the concentration effect which influences the competition between the formation of **int1** and **int11**. Based on the reaction rate equation, the reaction rate (r_1 and r_2) for the formation of **int1** and **int11** can be calculated by (Eqs 1, 2), respectively. Thus, their ratio (r_1/r_2) is determined by Eq. 3 which is affected by the ratio of rate constants (k_1/k_2) and the concentration ([$PhSiH_3$]/[BCF]). k_1/k_2 is calculated based on the Erying equation (Eq. 4)

$$r_1 = k_1[1a][PhSiH_3] \quad (1)$$

$$r_2 = k_2[1a][BCF] \quad (2)$$

$$\frac{r_1}{r_2} = \frac{k_1}{k_2}\frac{[PhSiH_3]}{[BCF]} \quad (3)$$

$$\frac{k_1}{k_2} = \frac{\frac{k_BT}{h}e^{-\frac{\Delta G_1^{\neq}}{RT}}}{\frac{k_BT}{h}e^{-\frac{\Delta G_2^{\neq}}{RT}}} = e^{-\frac{\Delta G_1^{\neq}-\Delta G_2^{\neq}}{RT}} \quad (4)$$

As the activation energy difference between **TS1** and **TS10** is 2.0 kcal/mol (Figure 5), k_1/k_2 is calculated to be 0.077 at 120°C. Therefore, r_1/r_2 for the reaction with equivalent amount of $PhSiH_3$ and $B(C_6F_5)_3$ is as small as 0.077, suggesting the

formation of **int11** is dominant. However, under the catalytic reaction condition with 20% mol of $B(C_6F_5)_3$ and 4 equivalents of $PhSiH_3$, the concentration ratio [$PhSiH_3$]/[BCF] increases to 20. As a result, r_1/r_2 is increased by 20 folds compared to that of the stoichiometric reaction with equivalent of $PhSiH_3$ and $B(C_6F_5)_3$, and thus the formation of **int1** is 1.54 times faster than **int11**. This result is in good agreement with the experimental observation that increasing the equivalent of $PhSiH_3$ gradually increases the yields of silylammonium borohydride intermediate and deamination product in the stoichiometric reaction with 1 equivalent of $B(C_6F_5)_3$. Therefore, the excess $PhSiH_3$ plays a crucial role to maintain a high [$PhSiH_3$]/[BCF] ratio so that $PhSiH_3$ can compete with $B(C_6F_5)_3$ for binding with the amine substrate, avoiding the deactivation of catalyst and substrate.

Reactivity of amines with different α-substitutions

In the original experimental work, control experiments were performed to assess the relative reactivity of a variety of benzylamines. As shown in Scheme 2, the competition reaction with one equivalent of an equimolar benzylamines mixture (**1b**, **1c**, **1d**) demonstrates that the relative reactivity of benzylamines follows the order: **1b** < **1c** < **1d**. To understand the relative reactivity of benzyl amines with different degrees of substitution at the α-carbon atom, we calculated the reaction pathway one for all substrates. Pathway one involves three main steps, i.e., the amine-silane binding, amine silylation, and deamination (Figure 6). It is worth noting that, for substrate **1d**, the silylation step (**TS2d**, $\Delta G^{\ddagger}$ = 26.2 kcal/mol) remains as the rate-limiting step, like the reaction with **1a**. However, for substrate **1b** and **1c**, the C–N bond cleavage of monosilylammonium borohydride (i.e., deamination) *via* **TS3b** ($\Delta G^{\ddagger}$ = 28.7 kcal/mol) and **TS3c** ($\Delta G^{\ddagger}$ = 27.2 kcal/mol) becomes the rate-determining step. Thus, the overall reaction energy barriers for the deamination of **1b/1c/1d** are calculated to be 28.7, 27.2 and 26.2 kcal/mol, respectively, which is consistent with the experimental observed reactivity order. Figure 6 clearly shows that the C–N bond cleavage (**TS3**) of **1d** is more favorable than **1b** and **1c**, which is because the reacting benzylic carbon in **TS3d** is stabilized by more methyl substituents, leading to stronger stabilization effect on the transition state.

Substituent effect of hydrosilanes

In the end, we turn our attention to the reactivity of hydrosilanes, another important reactant for the deamination reaction. To study the substituent effect of $PhSiH_3$, we calculated the reaction of a series of $PhSiH_3$ derivatives that carry electron-withdrawing groups (EWGs) or electron-donating groups (EDGs) at the phenyl ring. Figure 7 summarizes the Gibbs energies of all TSs of deamination reaction with different silanes ($PhSiH_3$, $C_6F_5SiH_3$, *1,3,5*-$C_6H_3F_2SiH_3$, *1,3,5*-$C_6H_3Cl_2SiH_3$, *1,3,5*-$C_6H_3Br_2SiH_3$, and *1,3,5*-$C_6H_3Me_2SiH_3$). In all reactions, the silylation step (**TS2**) is the rate-determining step. Compared to unsubstituted $PhSiH_3$, hydrosilanes with EWGs, such as F, Cl, and Br substituents, lower the barrier of **TS2** by 0.4–2.0 kcal/mol. Moreover, the formation of amine-silane complex (**TS1**) becomes more favorable than the generation of amine-boron Lewis product as **TS1** for the EWG-substituted hydrosilanes are lower in energy than **TS10** by 0.7–1.2 kcal/mol. This indicates that the reaction with these hydrosilanes may not need excess amount of silane reagent. The increased reactivity and binding affinity of hydrosilanes caused by the EWGs may because the EWGs increases the acidity of hydrosilanes which makes them more reactive toward amine substrates. On the contrary, EDGs will decrease the acidity of hydrosilane and thus lower the reactivity. Indeed, the potential energy surface of *1,3,5*-$C_6H_3Me_2SiH_3$ lies above the energy surface of $PhSiH_3$.

Conclusion

In the present study, we perform DFT calculations on the reaction of $B(C_6F_5)_3$-catalyzed reductive deamination of benzylic amines with hydrosilanes. Three possible reaction pathways (shown in Figure 1) involving mono-, bi- or tri-silylammonium borohydride as active intermediate were explored. The computational results reveal that the pathway one which includes the deamination of monosilylammonium borohydride is most favorable. Pathway one consists of three steps: first, amine and silane associate to form an amine-silane Lewis adduct; then, the amine-silane complex is catalyzed by $B(C_6F_5)_3$ to undergo silylation reaction, affording monosilylammonium borohydride intermediate; finally, the C–N dissociation of monosilylammonium borohydride intermediate generates the desired deamination product. The second step (silylation process) is the rate-determining step. The monosilylammonium borohydride prefers to undergo S_N2 C–N bond dissociation rather than the dehydrogenation, probably because the C–N is weaker than the N–H bond and the π-π stacking interaction stabilizes the transition state for C–N bond dissociation.

Our computational results suggest that $B(C_6F_5)_3$ acts as stronger Lewis acid than hydrosilane to bind with amine substrate, which will deactivate the catalyst and substrate. The excess silanes used in the experiment play an essential role to maintain a high concentration of silane which enables $PhSiH_3$ to compete with $B(C_6F_5)_3$ for binding with amine substrate, avoiding the deactivation of catalyst and substrate. Furthermore, the calculated relative reactivity of benzylamines with different degrees of substitution agrees well with the experimental observed reactivity order. In addition, our DFT studies on the substituent effect of silanes indicate that the introduction of electron-withdrawing groups on the phenyl ring of $PhSiH_3$ could lower the reaction energy barrier of the reductive

deamination reaction, which may improve the reaction efficiency. Overall, this work promotes the understanding of mechanism of deamination reaction and lays the theoretical foundation for the development of new deamination methodology.

Data availability statement

The original contributions presented in the study are included in the article/Supplementary Material, further inquiries can be directed to the corresponding author.

Author contributions

MZ and TW performed calculations and data analysis. G-JC designed the project and wrote the paper. All authors reviewed the manuscript.

Funding

This work is supported by the National Natural Science Foundation of China (no. 21803047), the Shenzhen Science and Technology Program (Grant No. RCYX20200714114736199), and the research grant from Shenzhen Key Laboratory Project (no. ZDSYS20190902093417963).

Conflict of interest

The authors declare that the research was conducted in the absence of any commercial or financial relationships that could be construed as a potential conflict of interest.

Publisher's note

Supplementary material

The Supplementary Material for this article can be found online at: https://www.frontiersin.org/articles/10.3389/fchem.2022.1025135/full#supplementary-material

SUPPLEMENTARY FIGURE S1
Gibbs energy profile for the B(C6F5)3-catalyzed reductive deamination with PhSiH3 and 1b/1c/1d by pathway 2.

SUPPLEMENTARY FIGURE S2
Frontier molecular orbital analysis of 1a, B(C6F5) and PhSiH3 (top) and the NCI surfaces of int1 and int11 (bottom).

SUPPLEMENTARY FIGURE S3
The formation of int12 and int13.

SUPPLEMENTARY FIGURE S4
Gibbs energy profile for the structural rearrangement between int2 and int4.

SUPPLEMENTARY FIGURE S5
Gibbs energy profile for the structural rearrangement between int6 and int8.

SUPPLEMENTARY TABLE S1
Corrections to zero point energies, enthalpies, free energies and electronic potential energies (in Hartree) and imaginary frequencies (IF) (cm-1) of optimized structures which were calculated at B3LYP-D3/def2-SVP//B3LYP-D3/def2-TZVP level in solvent (1,2- diflurobenzene) at 298.15 K and 393.15K and 1 atm.

References

Adduci, L. L., Bender, T. A., Dabrowski, J. A., and Gagné, M. R. (2015). Chemoselective conversion of biologically sourced polyols into chiral synthons. *Nat. Chem.* 7, 576–581. doi:10.1038/nchem.2277

Adduci, L. L., McLaughlin, M. P., Bender, T. A., Becker, J. J., and Gagné, M. R. (2014). Metal-free deoxygenation of carbohydrates. *Angew. Chem. Int. Ed.* 53, 1646–1649. doi:10.1002/anie.201306864

Adlington, M. G., Orfanopoulos, M., and Fry, J. L. (1976). A convenient one-step synthesis of hydrocarbons from alcohols through use of the organosilane-boron trifluoride reducing system. *Tetrahedron Lett.* 17, 2955–2958. doi:10.1016/s0040-4039(01)85498-8

Barluenga, J., Tomás-Gamasa, M., Aznar, F., and Valdés, C. (2009). Metal-free carbon–carbon bond-forming reductive coupling between boronic acids and tosylhydrazones. *Nat. Chem.* 1, 494–499. doi:10.1038/nchem.328

Reductive deaminative conversion involving isonitrilation-reduction: Barton, D. H. R., Bringmann, G., Lamotte, G., Motherwell, W. B., Hay Motherwell, R. S., and Porter, A. E. A. (1980). *J. Chem. Soc. Perkin Trans.* 1, 2657–2664.

Barton, D. H. R., Jang, d. O., and Jaszberenyi, J. Cs. (1992). *Tetrahedron Lett.* 33, 5709–5712.

Becke, A. D. (1993). Density-functional thermochemistry. III. The role of exact exchange. *J. Chem. Phys.* 98, 5648–5652. doi:10.1063/1.464913

Bender, T. A., Dabrowski, J. A., and Gagné, M. R. (2016). Delineating the multiple roles of $B(C_6F_5)_3$ in the chemoselective deoxygenation of unsaturated polyols. *ACS Catal.* 6, 8399–8403. doi:10.1021/acscatal.6b02551

Bender, T. A., Dabrowski, J. A., Zhong, H., and Gagné, M. R. (2016). Diastereoselective $B(C_6F_5)_3$-catalyzed reductive carbocyclization of unsaturated carbohydrates. *Org. Lett.* 18, 4120–4123. doi:10.1021/acs.orglett.6b02050

Chatterjee, I., Porwal, D., and Oestreich, M. (2017). $B(C_6F_5)_3$-Catalyzed chemoselective defunctionalization of ether-containing primary alkyl tosylates with hydrosilanes. *Angew. Chem. Int. Ed.* 56, 3389–3391. doi:10.1002/anie.201611813

Cheng, G., Drosos, N., Morandi, B., and Thiel, W. (2018). Computational study of $B(C_6F_5)_3$-catalyzed selective deoxygenation of 1, 2-diols: Cyclic and noncyclic pathways. *ACS Catal.* 8, 1697–1702. doi:10.1021/acscatal.7b04209

Corma, A., Iborra, S., and Velty, A. (2007). Chemical routes for the transformation of biomass into chemicals. *Chem. Rev.* 107, 2411–2502. doi:10.1021/cr050989d

Correia, J. T. M., Fernandes, V. A., Matsuo, B. T., Delgado, J. A. C., de Souza, W. C., and Paixão, M. W. (2020). *Chem. Commun.* 56 (4), 503–514.

Dai, X., and Li, C. (2016). En route to a practical primary alcohol deoxygenation. *J. Am. Chem. Soc.* 138, 5433–5440. doi:10.1021/jacs.6b02344

Doyle, M. P., West, T. C., Donnelly, J. S., and McOsker, C. C. (1976). Silane reductions in acidic media. *J. Organomet. Chem.* 117, 129–140. doi:10.1016/s0022-328x(00)87264-2

Drosos, N., Cheng, G., Ozkal, E., Cacherat, B., Thiel, W., and Morandi, B. (2017). Catalytic reductive pinacol-type rearrangement of unactivated 1, 2-diols through a concerted, stereoinvertive mechanism. *Angew. Chem. Int. Ed.* 56, 13377–13381. doi:10.1002/anie.201704936

Drosos, N., and Morandi, B. (2015). Boron-catalyzed regioselective deoxygenation of terminal 1, 2-diols to 2-alkanols enabled by the strategic formation of a cyclic siloxane intermediate. *Angew. Chem. Int. Ed.* 54, 8814–8818. doi:10.1002/anie.201503172

Drosos, N., Ozkal, E., and Morandi, B. (2016). *Synlett* 27, 1760–1764.

Fang, H., and Oestreich, M. (2020). Defunctionalisation catalysed by boron Lewis acids. *Chem. Sci.* 11, 12604–12615. doi:10.1039/d0sc03712e

Fang, H., and Oestreich, M. (2020). Reductive deamination with hydrosilanes catalyzed by $B(C_6F_5)_3$. *Angew. Chem. Int. Ed.* 59, 11394–11398. doi:10.1002/anie.202004651

Frisch, M. J., Trucks, G. W., Schlegel, H. B., Scuseria, G. E., Robb, M. A., Cheeseman, J. R., et al. (2016). *Gaussian 16, revision A.03.* Wallingford CT: Gaussian, Inc.

Geoffroy, O. J., Morinellib, T. A., and Meier, G. P. (2001). Chemoselective one-pot reductive deamination of aryl amines. *Tetrahedron Lett.* 42, 5367–5369. doi:10.1016/s0040-4039(01)01027-9

Gevorgyan, V., Liu, J., Rubin, M., Benson, S., and Yamamoto, Y. (1999). A novel reduction of alcohols and ethers with a HSiEt3catalytic B(C6F5)3 system. *Tetrahedron Lett.* 40, 8919–8922. doi:10.1016/s0040-4039(99)01757-8

Gevorgyan, V., Rubin, M., Benson, S., Liu, J., and Yamamoto, Y. (2000). A novel $B(C_6F_5)_3$-catalyzed reduction of alcohols and cleavage of aryl and alkyl ethers with hydrosilanes. *J. Org. Chem.* 65, 6179–6186. doi:10.1021/jo000726d

Gevorgyan, V., Rubin, M., Liu, J., and Yamamoto, Y. (2001). A direct reduction of aliphatic aldehyde, acyl chloride, ester, and carboxylic functions into a methyl group. *J. Org. Chem.* 66, 1672–1675. doi:10.1021/jo001258a

Gonzalez, C., and Gonzalez, H. B. (1990). Reaction path following in mass-weighted internal coordinates. *J. Phys. Chem.* 94, 5523–5527. doi:10.1021/j100377a021

Greb, L., Tamke, S., and Paradies, J. (2014). Catalytic metal-free Si–N cross-dehydrocoupling. *Chem. Commun.* 50, 2318–2320. doi:10.1039/c3cc49558b

Grimme, S., Ehrlich, S., and Goerigk, L. J. (2011). Effect of the damping function in dispersion corrected density functional theory. *J. Comput. Chem.* 32, 1456–1465. doi:10.1002/jcc.21759

Grimme, S. (2019). Exploration of chemical compound, conformer, and reaction space with meta-dynamics simulations based on tight-binding quantum chemical calculations. *J. Chem. Theory Comput.* 15, 2847–2862. doi:10.1021/acs.jctc.9b00143

Hermeke, J., Mewald, M., and Oestreich, M. (2013). Experimental analysis of the catalytic cycle of the borane-promoted imine reduction with hydrosilanes: Spectroscopic detection of unexpected intermediates and a refined mechanism. *J. Am. Chem. Soc.* 135, 17537–17546. doi:10.1021/ja409344w

Hu, J., Wang, G., Li, Sh., and Shi, Zh. (2018). Selective C–N borylation of alkyl amines promoted by Lewis base. *Angew. Chem. Int. Ed.* 57, 15227–15231. doi:10.1002/anie.201809608

Huber, G. W., Iborra, S., and Corma, A. (2006). Synthesis of transportation fuels from Biomass: chemistry, catalysts, and engineering. *Chem. Rev.* 106, 4044–4098. doi:10.1021/cr068360d

Humphrey, W., Dalke, A., and Schulten, K. (1996). VMD: Visual molecular dynamics. *J. Mol. Graph.* 14, 33–38. doi:10.1016/0263-7855(96)00018-5

Lee, C., Yang, W., and Parr, R. G. (1988). Development of the Colle-Salvetti correlation-energy formula into a functional of the electron density. *Phys. Rev. B* 37, 785–789. doi:10.1103/physrevb.37.785

Legault, C. Y. (2009). *CYLview, 1.0b*. Sherbrooke, Canada: Université de Sherbrooke. Available at: http://www.cylview.org.

Lu, T., and Chen, F. (2012). Multiwfn: A multifunctional wavefunction analyzer. *J. Comput. Chem.* 33, 580–592. doi:10.1002/jcc.22885

Marenich, A. V., Cramer, C. J., and Truhlar, D. G. (2009). Universal solvation model based on solute electron density and on a continuum model of the solvent defined by the bulk dielectric constant and atomic surface tensions. *J. Phys. Chem. B* 113, 6378–6396. doi:10.1021/jp810292n

Massad, G., Zhao, H., and Mobley, H. L. (1995). *Proteus mirabilis* amino acid deaminase: Cloning, nucleotide sequence, and characterization of aad. *J. Bacteriol.* 177, 5878–5883. doi:10.1128/jb.177.20.5878-5883.1995

McLaughlin, M. P., Adduci, L. L., Becker, J. J., and Gagne, M. R. (2013). Iridium-catalyzed hydrosilylative reduction of glucose to hexane(s). *J. Am. Chem. Soc.* 135, 1225–1227. doi:10.1021/ja3110494

Reductive deaminative conversion involving or diazotization-dediazotization: Mitsuhashi, H., Kawakami, T., and Suzuki, H. (2000). *Tetrahedron Lett.* 41, 5567–5569.

Molla, G., Melis, R., and Pollegioni, L. (2017). Breaking the mirror: l-Amino acid deaminase, a novel stereoselective biocatalyst. *Biotechnol. Adv.* 35, 657–668. doi:10.1016/j.biotechadv.2017.07.011

Katritzky salts as intermediate to construct for C-C, C-B and C-S bond: Ni, S., Li, C., Mao, Y., Han, J., Wang, Y., Yan, H., et al. (2019). Ni-catalyzed deaminative cross-electrophile coupling of Katritzky salts with halides via C─N bond activation. *Sci. Adv.* 5, 1–5. doi:10.1126/sciadv.aaw9516

Nikolaos Drosos, M. Sc., and Morandi, B. (2015). Boron-catalyzed regioselective deoxygenation of terminal 1, 2-diols to 2-alkanols enabled by the strategic formation of a cyclic siloxane intermediate. *Angew. Chem. Int. Ed.* 54, 8814–8818. doi:10.1002/anie.201503172

Nimmagadda, R. D., and McRae, C. (2006). A novel reduction reaction for the conversion of aldehydes, ketones and primary, secondary and tertiary alcohols into their corresponding alkanes. *Tetrahedron Lett.* 47, 5755–5758. doi:10.1016/j.tetlet.2006.06.007

Nshimiyimana, P., Liu, L., and Du, G. (2019). Engineering of L-amino acid deaminases for the production of α-keto acids from L-amino acids. *Bioengineered* 10, 43–51. doi:10.1080/21655979.2019.1595990

Orfanopoulos, M., and Smonou, I. (1988). Selective reduction of diaryl or aryl alkyl alcohols in the presence of primary hydroxyl or ester groups by etherated boron trifluoride-triethylsilane system. *Synth. Commun.* 18, 833–839. doi:10.1080/00397918808057852

Pang, Y., Moser, D., and Cornella, J. (2020). Pyrylium salts: Selective reagents for the activation of primary amino groups in organic synthesis. *Synthesis* 52, 489–503. doi:10.1055/s-0039-1690703

Peng, C., Zhang, W., Yan, G., and Wang, J. (2009). Arylation and vinylation of α-diazocarbonyl compounds with boroxines. *Org. Lett.* 11, 1667–1670. doi:10.1021/ol900362d

Petersen-Mahrt, S. K., Coker, H. A., and Pauklin, S. (2009). DNA deaminases: AIDing hormones in immunity and cancer. *J. Mol. Med.* 87, 893–897. doi:10.1007/s00109-009-0496-6

Richter, S. C., and Oestreich, M. (2021). Chemoselective deoxygenation of 2° benzylic alcohols through a sequence of formylation and $B(C_6F_5)_3$-catalyzed reduction. *Eur. J. Org. Chem.* 2021, 2103–2106. doi:10.1002/ejoc.202100148

Schafer, A., Horn, H., and Ahlrichs, R. (1992). Fully optimized contracted Gaussian basis sets for atoms Li to Kr. *J. Chem. Phys.* 97, 2571–2577. doi:10.1063/1.463096

Schafer, A., Huber, C., and Ahlrichs, R. (1994). Fully optimized contracted Gaussian basis sets of triple zeta valence quality for atoms Li to Kr. *J. Chem. Phys.* 100, 5829–5835. doi:10.1063/1.467146

Seo, Y., and Gagné, M. R. (2018). Positional selectivity in the hydrosilylative partial deoxygenation of disaccharides by boron catalysts. *ACS Catal.* 8, 81–85. doi:10.1021/acscatal.7b02992

Seo, Y., Gudz, A., Lowe, J. M., and Gagné, M. R. (2019). Selective deoxygenation of gibberellic acid with fluoroarylborane catalysts. *Tetrahedron* 75, 130712–130720. doi:10.1016/j.tet.2019.130712

Vesely, C., Tauber, S., Sedlazeck, F. J., von Haeseler, A., and Jantsch, M. F. (2012). Adenosine deaminases that act on RNA induce reproducible changes in abundance and sequence of embryonic miRNAs. *Genome Res.* 22, 1468–1476. doi:10.1101/gr.133025.111

Wang, X., Kuang, Y., Ye, S., and Wu, J. (2019). Photoredox-catalyzed synthesis of sulfones through deaminative insertion of sulfur dioxide. *Chem. Commun.* 55, 14962–14964. doi:10.1039/c9cc08333b

Wu, G., Deng, Y., Wu, C., Wang, X., Zhang, Y., and Wang, J. (2014). Switchable 2, 2, 2-trifluoroethylation and*gem*-difluorovinylation of organoboronic acids with 2, 2, 2-trifluorodiazoethane. *Eur. J. Org. Chem.* 21, 4477–4481. doi:10.1002/ejoc.201402597

Yasuda, M., Onishi, Y., Ueba, M., Miyai, T., and Baba, A. (2001). Direct reduction of Alcohols: highly chemoselective reducing system for secondary or tertiary alcohols using chlorodiphenylsilane with a catalytic amount of indium trichloride. *J. Org. Chem.* 66, 7741–7744. doi:10.1021/jo0158534

Zhang, J., Park, S., and Chang, S. (2018). Catalytic access to bridged sila-*N*-heterocycles from piperidines via cascade sp^3 and sp^2 C–Si bond formation. *J. Am. Chem. Soc.* 140, 13209–13213. doi:10.1021/jacs.8b08733

Zhang, Z., Song, J., and Han, B. (2017). Catalytic transformation of lignocellulose into chemicals and fuel products in ionic liquids. *Chem. Rev.* 117, 6834–6880. doi:10.1021/acs.chemrev.6b00457

Zhou, C. H., Xia, X., Lin, C. X., Tong, D. S., and Beltramini, J. (2011). Catalytic conversion of lignocellulosic biomass to fine chemicals and fuels. *Chem. Soc. Rev.* 40, 5588–5617. doi:10.1039/c1cs15124j

Zhou, M., Park, S., and Dang, L. (2020). Dual reactivity of $B(C_6F_5)_3$ enables the silylative cascade conversion of *N*-aryl piperidines to sila-N-heterocycles: DFT calculations. *Org. Chem. Front.* 7, 944–952. doi:10.1039/c9qo01437c